

# Geophysical Research Letters<sup>®</sup>



## RESEARCH LETTER

10.1029/2023GL105773

Stephen P. Hicks and Sandro B. Matos  
contributed equally to this work.

### Key Points:

- We use seismic and infrasound data to characterize a previously unreported fireball over the North Atlantic Ocean in June 2022
- The fireball was detected by the Geostationary Lightning Mapper onboard the GOES-16 satellite, giving a precise constraint on blast time
- Seismoacoustic data, in tandem with satellite observations, can help to improve our observational completeness of near-Earth objects

### Supporting Information:

Supporting Information may be found in the online version of this article.

### Correspondence to:

S. P. Hicks,  
[stephen.hicks@ucl.ac.uk](mailto:stephen.hicks@ucl.ac.uk)

### Citation:

Hicks, S. P., Matos, S. B., Pimentel, A., Belli, G., Gheri, D., Tsekhmistrenko, M., et al. (2023). Exclusive seismoacoustic detection and characterization of an unseen and unheard fireball over the North Atlantic. *Geophysical Research Letters*, 50, e2023GL105773. <https://doi.org/10.1029/2023GL105773>

Received 9 AUG 2023  
Accepted 25 OCT 2023

### Author Contributions:

**Conceptualization:** Stephen P. Hicks, Sandro B. Matos, Adriano Pimentel, Maria Tsekhmistrenko, Kasra Hosseini, Ana M. G. Ferreira

**Data curation:** Stephen P. Hicks, Sandro B. Matos, Adriano Pimentel, Giacomo Belli, Duccio Gheri, Maria Tsekhmistrenko, Kasra Hosseini, Wolfram H. Geissler, Rita Silva, Nicolau Wallenstein, Ana M. G. Ferreira

© 2023. The Authors.

This is an open access article under the terms of the [Creative Commons Attribution License](https://creativecommons.org/licenses/by/4.0/), which permits use, distribution and reproduction in any medium, provided the original work is properly cited.

## Exclusive Seismoacoustic Detection and Characterization of an Unseen and Unheard Fireball Over the North Atlantic

Stephen P. Hicks<sup>1</sup> , Sandro B. Matos<sup>2</sup> , Adriano Pimentel<sup>2,3</sup> , Giacomo Belli<sup>4</sup> , Duccio Gheri<sup>4</sup> , Maria Tsekhmistrenko<sup>1</sup>, Kasra Hosseini<sup>1</sup>, Wolfram H. Geissler<sup>5</sup> , Rita Silva<sup>2,3</sup> , Nicolau Wallenstein<sup>2</sup> , and Ana M. G. Ferreira<sup>1</sup> 

<sup>1</sup>Department of Earth Sciences, University College London, London, UK, <sup>2</sup>Instituto de Investigação em Vulcanologia e Avaliação de Riscos (IVAR), Universidade dos Açores, Azores, Portugal, <sup>3</sup>Centro de Informação e Vigilância Sismovulcânica dos Açores (CIVISA), Azores, Portugal, <sup>4</sup>Dipartimento di Scienze della Terra, Università degli Studi di Firenze, Firenze, Italy, <sup>5</sup>Alfred Wegener Institute, Helmholtz Centre for Polar and Marine Research, Bremerhaven, Germany

**Abstract** Small meteoroids that enter Earth's atmosphere often go unnoticed because their detection and characterization rely on human observations, introducing observational biases in space and time. Acoustic shockwaves from meteoroid ablation convert to infrasound and seismic energy, enabling fireball detection using seismoacoustic methods. We analyzed an unreported fireball in 2022 near the Azores, recorded by 26 seismometers and two infrasound arrays. Through polarization analyses, array methods, and 3-D ray-tracing, we determined that the terminal blast occurred at 40 km altitude, ~60 km NE of São Miguel Island. This location matches an unidentified flash captured by a lightning detector aboard the GOES-16 satellite. The estimated kinetic energy is  $\sim 10^{-3}$  kT TNT equivalent, suggesting a  $10^{-1}$  m object diameter, thousands of which enter the atmosphere annually. Our results demonstrate how geophysical methods, in tandem with satellite data, can significantly improve the observational completeness of meteoroids, advancing our understanding of their sources and entry processes.

**Plain Language Summary** Every year, hundreds to thousands of small near-Earth objects, known as meteoroids, enter Earth's atmosphere. Their hypersonic entry speed and break-up can generate flashes known as fireballs and associated shockwaves that can reach the ground. However, it is only the largest objects breaking up above populated areas that we typically see or hear, or that are captured by dedicated camera systems. Many of the smaller meteoroids go unnoticed. This observational bias limits our understanding of these objects and how they enter Earth's atmosphere. Here, we report on a fireball that broke up over the Northern Atlantic Ocean in June 2022 and was recorded on a network of seismometers that record sensitive ground motion and infrasound sensors that “hear” low-frequency sound waves. Our analyses of these data show a small (40 cm diameter) meteoroid exploded at around 40 km altitude and 60 km northeast of São Miguel Island. Crucially, a flash recorded by a lightning mapper aboard a weather satellite provides us with the exact time of the explosion. To the best of our knowledge, this event is one of few documented cases of a fireball detected solely by geophysical means without relying on initial reports from human observers or photographic/video evidence.

## 1. Introduction

Meteors provide valuable insights into the solar system's early history and chemical composition. These objects travel at speeds of 11–74 km/s (Ceplecha et al., 1998; Drolshagen et al., 2020), creating fireballs when they explode upon entering the atmosphere. Bright flashes are often seen by people and captured on dedicated *all-sky* cameras or more general-purpose equipment such as CCTV systems and dash-cams. Large (>1 m diameter) meteoroids, which enter Earth's atmosphere biweekly on average (Rumpf et al., 2019), generate shockwaves and an audible boom. These shockwaves, which convert into acoustic energy (Revelle, 1976), are caused by the meteoroid's high-speed atmospheric entry or by its catastrophic fragmentation, resulting in different wave propagation effects (Edwards et al., 2008).

Acoustic and coupled seismic energy from falling meteoroids can be recorded by infrasound and seismic sensors (Brown et al., 2003; D'Auria et al., 2006; Edwards et al., 2008; Ishihara et al., 2003; Langston, 2004; Pujol et al., 2005, 2006; Stich et al., 2022; Tatum, 1999; Vera Rodriguez et al., 2022; Yamada, 2021). Infrasound sensors typically record characteristic *N*-waves (Kanamori et al., 1991), whereas velocity records are *W*-shaped (D'Auria

**Formal analysis:** Stephen P. Hicks, Sandro B. Matos, Adriano Pimentel, Giacomo Belli, Duccio Gheri, Ana M. G. Ferreira

**Funding acquisition:** Nicolau Wallenstein, Ana M. G. Ferreira

**Investigation:** Stephen P. Hicks, Sandro B. Matos, Adriano Pimentel, Giacomo Belli, Duccio Gheri, Maria Tsekhmistrenko, Kasra Hosseini, Wolfram H. Geissler, Nicolau Wallenstein, Ana M. G. Ferreira

**Methodology:** Stephen P. Hicks, Sandro B. Matos, Adriano Pimentel, Giacomo Belli, Duccio Gheri

**Project Administration:** Stephen P. Hicks, Ana M. G. Ferreira

**Resources:** Stephen P. Hicks, Sandro B. Matos, Adriano Pimentel, Wolfram H. Geissler, Rita Silva, Nicolau Wallenstein, Ana M. G. Ferreira

**Software:** Stephen P. Hicks, Sandro B. Matos, Giacomo Belli, Duccio Gheri

**Supervision:** Nicolau Wallenstein, Ana M. G. Ferreira

**Validation:** Stephen P. Hicks, Sandro B. Matos, Adriano Pimentel, Giacomo Belli, Duccio Gheri, Wolfram H. Geissler

**Visualization:** Stephen P. Hicks

**Writing – original draft:** Stephen P. Hicks, Sandro B. Matos, Adriano Pimentel, Giacomo Belli, Duccio Gheri, Ana M. G. Ferreira

**Writing – review & editing:** Stephen P. Hicks, Sandro B. Matos, Adriano Pimentel, Giacomo Belli, Duccio Gheri, Maria Tsekhmistrenko, Kasra Hosseini, Wolfram H. Geissler, Rita Silva, Nicolau Wallenstein, Ana M. G. Ferreira

et al., 2006; Langston, 2004). These data can help reconstruct the meteoroid's blast position and its trajectory. Two main methods are commonly used. One assumes straight rays and a constant velocity of sound through the atmosphere (Ishihara et al., 2003; Kumar et al., 2017; Langston, 2004; Pujol et al., 2006; Yamada, 2021; Yamada & Mori, 2012). The other involves ray-tracing in realistic atmospheric models while accounting for wind effects (Walker et al., 2010) to reconstruct the acoustic raypath in the atmosphere (Brown et al., 2003; Hedlin et al., 2010; Stich et al., 2022). However, distinguishing point sources from moving sources is challenging, particularly with limited observations (Vera Rodriguez et al., 2022). Other factors that complicate the modeling of seismoacoustic observations include multipathing, ground-coupled precursory signals, and site effects generating variable signal durations (Stich et al., 2022).

Studies on meteoroids primarily rely on initial visual and/or audible human observations (Brown, ReVelle, et al., 2002; Brown et al., 2003, 2011; D'Auria et al., 2006; Hughes et al., 2022; Ishihara et al., 2003; Kumar et al., 2017; Langston, 2004; Llorca et al., 2005; Pujol et al., 2005; Stich et al., 2022; Vera Rodriguez et al., 2022; Walker et al., 2010; Yamada, 2021; Yamada & Mori, 2012), leading to an observational bias toward populated areas, such as on the continents. Observations over oceans and islands are notably scarce, particularly without *all-sky* cameras (Silber & Brown, 2014). Factors like time of day and weather conditions can also limit human observations and camera recordings. However, new satellite sensors can identify flashes caused by fireballs (Jenniskens et al., 2018; Rumpf et al., 2019), addressing some spatial-temporal biases in data collection.

On 29 June 2022, routine visual inspection of waveforms from stations in the seismic network of the Centre for Information and Seismovolcanic Surveillance of the Azores (CIVISA) reported seismic signals across the island of São Miguel at 02:06 UTC. The slow moveout of these signals eliminated an earthquake or quarry blast source (the latter highly unlikely during the night). Anomalous signals were also detected on infrasonic arrays on the islands of Graciosa and São Jorge, ~200 km to the NW of São Miguel, some 10 min later. However, no one had reported visual or audible observations. We further searched social media and explored the possibility of obtaining webcam footage; however, we found no reports of fireballs. The local astronomical observatory Observatório Astronómico de Santana, Açores, located on the North coast of São Miguel also had no records of the event. Skies were clear that night, as confirmed by an infrared satellite image at 02:00 UTC (Figure S1 in Supporting Information S1).

Here, we study this suspected but previously unreported fireball in the Azores region using seismological, infrasonic, and satellite data. The implications of our study could enhance global data sets of near-Earth objects, thus presenting new opportunities for improving our understanding of these phenomena.

## 2. Seismic Data and Waveform Characteristics

To investigate this event, we analyzed all available seismic data from the Azores, primarily from CIVISA, the Azores seismo-volcanic monitoring agency (network code: CP) and the Portuguese National Seismic Network (network code: PM) (Instituto Português do Mar e da Atmosfera, I.P., 2006) (Figure 1a). These networks comprise a combination of single-component short-period, three-component short-period, and three-component broadband seismometers. Manual assessment of the waveforms shows that all but one of the 23 stations on São Miguel (Figures 1b and 2a) recorded the event.

We picked arrival times at the onset of the impulsive, higher frequency and higher-amplitude waveform peak. The earliest arrival was at station PM.BART on the East coast of São Miguel, with progressively later arrivals toward the West (Figure 1b). Concentric isochrones emanate from NE São Miguel (Figure 1b). We estimated the direction of the source using polarisation analysis, assuming the seismic signals likely originated from an incident acoustic wave (Langston, 2004), with most stations showing elliptical horizontal particle motions (Figure 2a). We computed polarisation azimuths (Flinn, 1965) from a window commencing at the picked onset time that captures the highest amplitude arrivals (~2 s for most stations), within the frequency range of 2–6 Hz, with 1 s windows overlapping every 0.1 s. Stations in East São Miguel have NE azimuths, while stations to the West and North have ENE-directed azimuths (Figure 1b). These directions are roughly perpendicular to the nearest isochrones and consistent with a source located NE of São Miguel. Less clear polarizations (e.g., at station CP.PGRON) likely result from precursory onsets (see below) or from the fixed window length used for the polarisation analysis.

Many of the seismic waveforms exhibit a *W*-shape (i.e., with downward first-motions) (Figure 2a), which is characteristic of a pressure *N*-wave on a velocity trace, suggesting a hypersonic or supersonic source (D'Auria

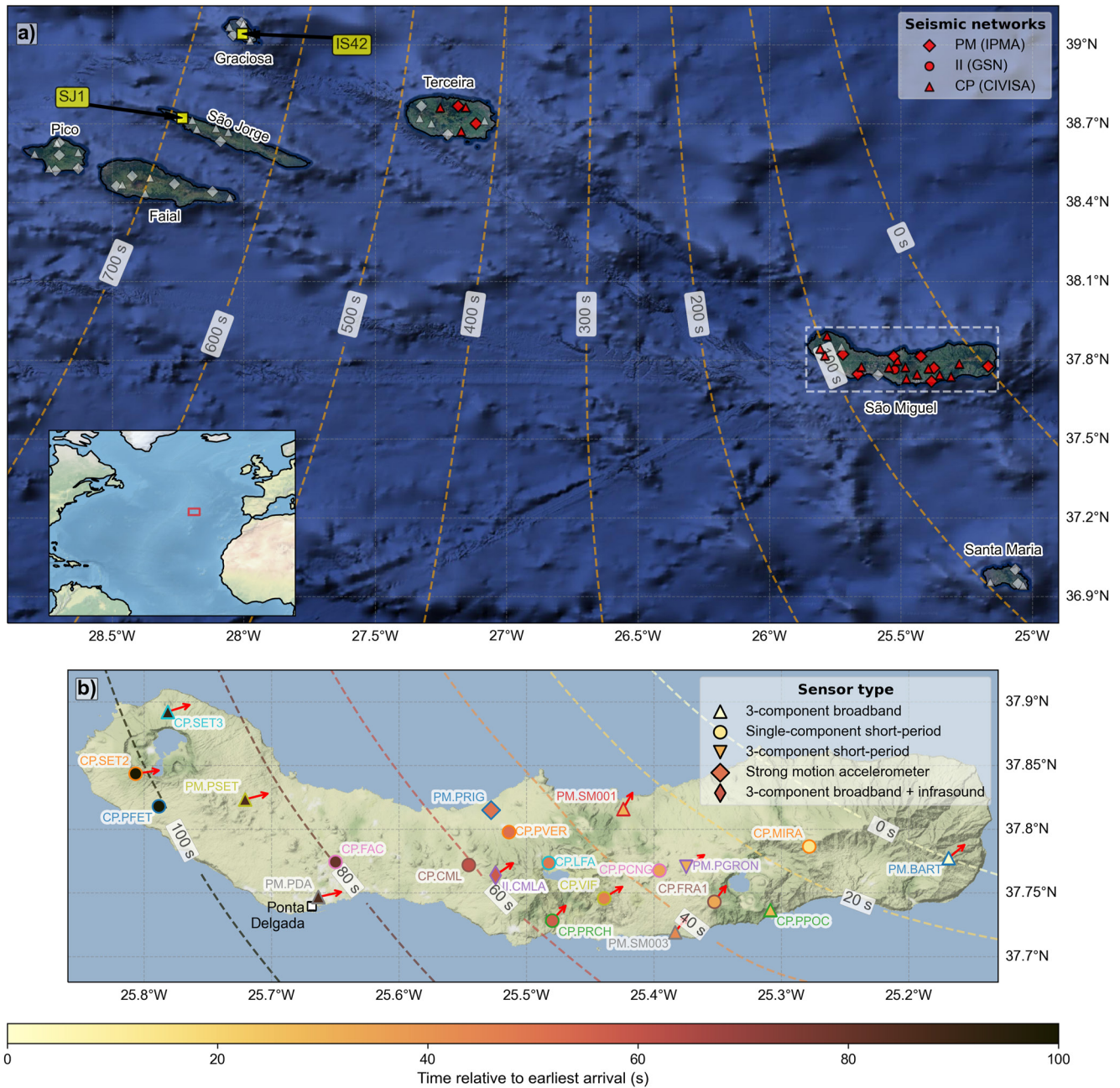


**Figure 1.** (a) Map of the central and eastern islands of the Azores (Pico, Faial, São Jorge, Graciosa, Terceira, São Miguel, and Santa Maria) showing seismic stations (triangles) and infrasound stations/arrays (yellow squares). Positive fireball detections are in red; negative detections are in white. Orange dashed contour lines represent interpolated relative isochrons using continuous curvature splines relative to the first arrival at PM.BART. The inset map shows the extent of the main map (red box) in the North Atlantic Ocean. The white dashed line shows the spatial extent of (b). (b) Map of seismic stations on São Miguel Island that recorded the shockwave arrival. Station labels and symbol outlines correspond to those in Figure 2. Station symbol fills are color-coded according to their arrival time relative to the first arrival at PM.BART. Red arrows indicate the best-fitting source azimuth from polarisation analysis (Flinn, 1965).

et al., 2006; Ishihara et al., 2003). The recorded signal is strongest in the frequency range of 1.5–8.0 Hz (Figure 2a), with less signal at audible frequencies (>20 Hz). There are substantial variations in waveform characteristics across São Miguel. The peak ground velocities vary greatly (Figure 2a). Signal durations also vary widely, ranging from 1.5 s at PM.PGRON to 18.4 s at CP.FAC (Figure 2a). Some waveforms appear highly monochromatic (e.g., CP.PVER), while others show hints of dispersion (e.g., PM.SM001). Most stations are installed on fractured lava flows or unconsolidated pumice deposits, which may explain the peak velocity frequency of ~3 Hz. Yet,



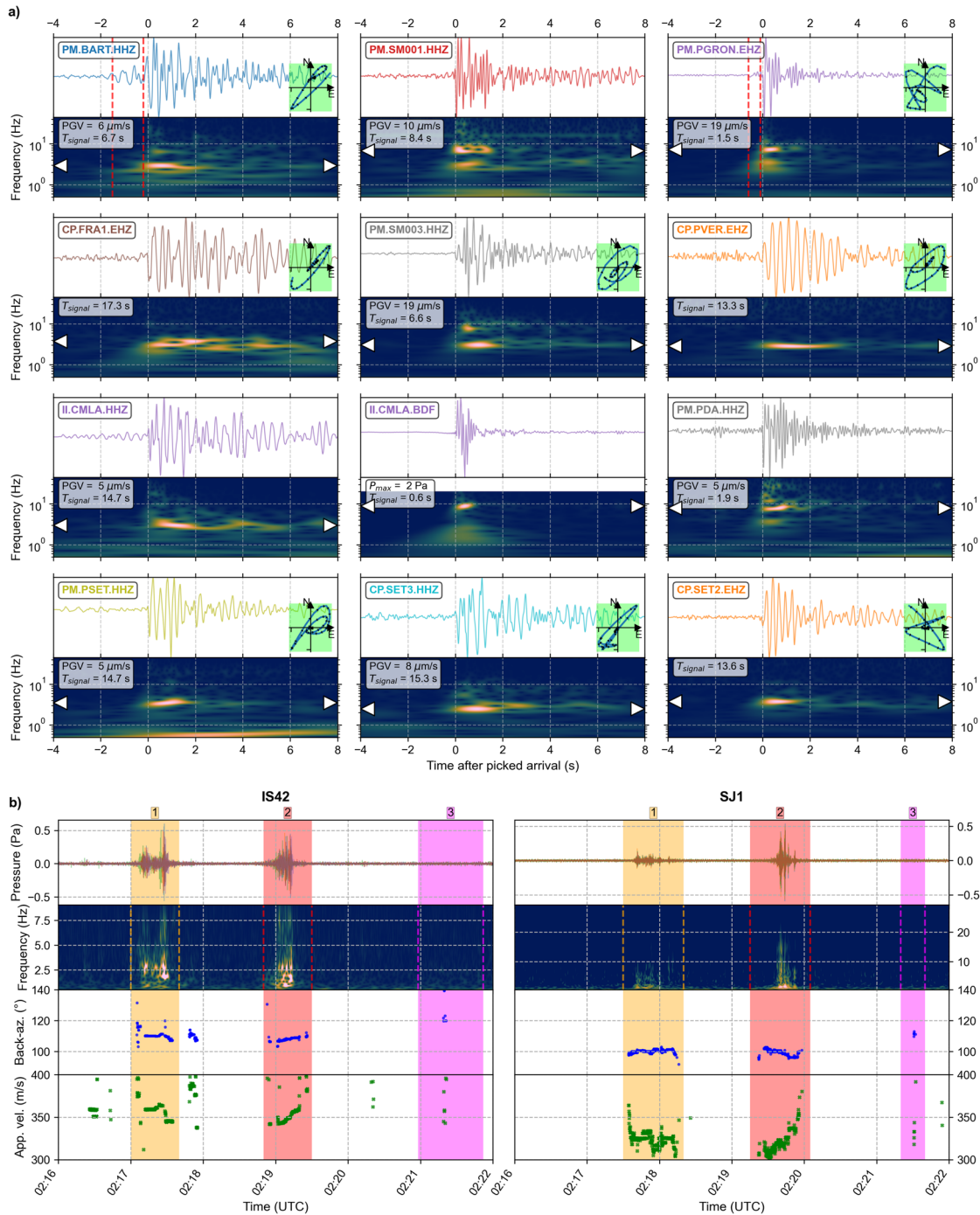


**Figure 2.** (a) Z-component seismic waveforms from São Miguel (filtered 1.5–12 Hz) and infrasound waveform of IL.CMLA.BDF (0.5 Hz highpass), with spectrograms below. Colors correspond to Figure 1. Green insets display horizontal particle motions in 0.7 s windows. The frequency at peak-ground velocity is indicated by white arrowheads. Signal duration, defined by 20% of the peak waveform envelope amplitude (Stich et al., 2022) is provided. Precursory signals on PM.BART & PM.PGRON are marked by vertical red lines. (b) Infrasound waveforms with computed array parameters. Three distinct signals are represented by colored strips.

we found no numerical correlation between waveform characteristics and station location, underlying geology, or elevation.

We only found obvious seismic signals from São Miguel Island, which aligns with previous observations of similar events within a limited area of  $\sim 100$  km<sup>2</sup> (D’Auria et al., 2006; Stich et al., 2022). However, we found weak signals with low signal-to-noise ratios at four stations on Terceira Island,  $\sim 150$  km to the NW (Figure 1a), with

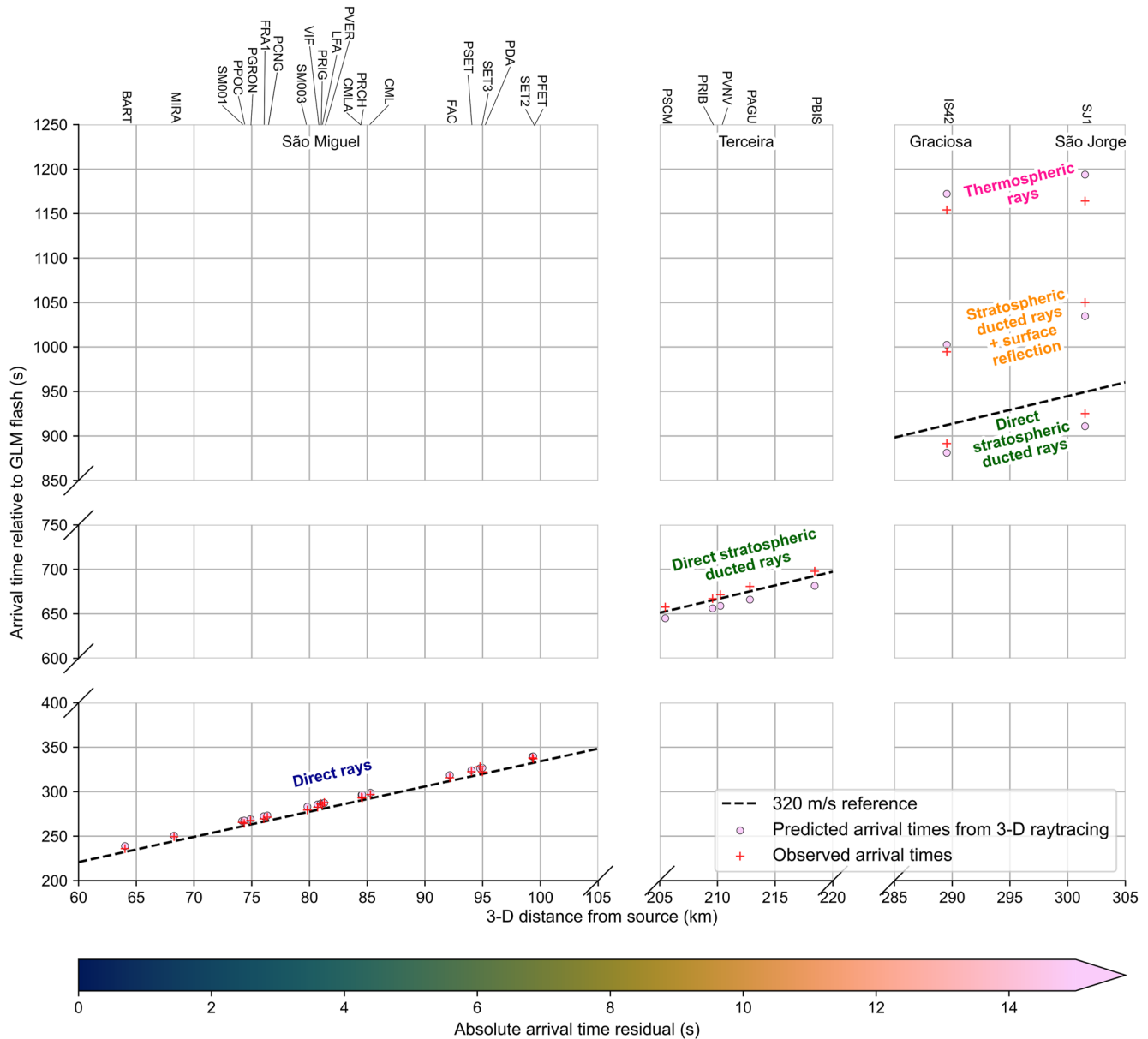


**Figure 3.** Observed versus predicted arrival time moveout using 3-D ray-tracing (Figure 4b) relative to the origin time constrained by the flash detected by the Geostationary Lightning Mapper. The source position comes from 3-D ray-tracing of infrasound array data. Predicted arrival times are colored according to their residuals. Station labels are given along the top.

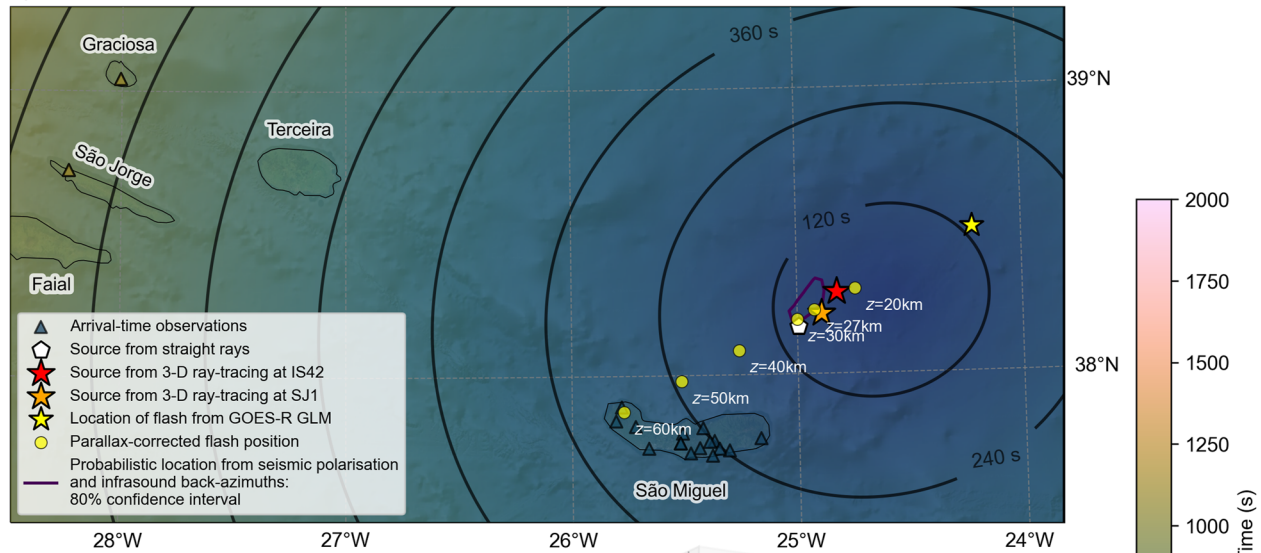
arrival times consistent with the moveout velocity observed elsewhere (Figure 3). Two stations on São Miguel (PM.BART; PM.PGRON) recorded a low-frequency precursory emergent onset lasting 0.5–1.5 s (Figure 2a).

### 3. Infrasound Observations and Array Processing

We analyzed data from multiple infrasound stations in the Azores (Figure 1a). The event was captured by the IS42 infrasonic array of the Comprehensive Nuclear-Test-Ban Treaty Organisation's (CTBTO's) International Monitoring System on Graciosa Island, by a portable infrasonic array (SJ1) installed on São Jorge Island, as well as by a single infrasound sensor (II.CMLA) collocated with a seismometer on São Miguel. For further information about these arrays, refer to Text S1 in Supporting Information S1.

At II.CMLA, a short duration (~1 s) high-frequency (~10 Hz) infrasound signal with a maximum peak-to-peak amplitude of 2.9 Pa is observed (Figure 2a). However, the wavetrain is internally complex (Silber & Brown, 2014),

a) Constant velocity, straight-rays



b) 3-D ray-tracing

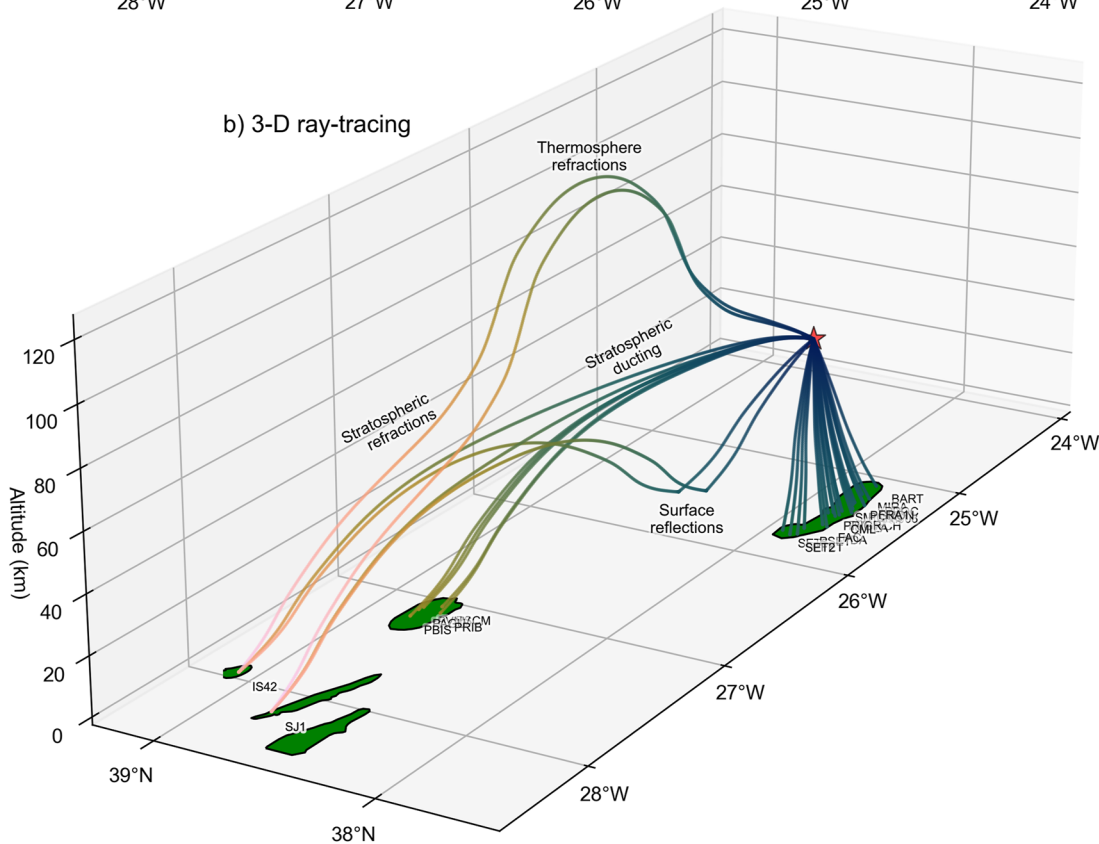


**Figure 4.** Meteoroid source models. (a) Source position assuming straight rays in a constant velocity medium, with concentric contours representing the predicted arrival times. (b) Perspective view from the SW of the source position derived using infrasound array data, displaying the 3-D raypaths traced in a realistic atmosphere model (colored by time).

consisting of at least four *N*-wave cycles, potentially superimposed onto a longer-period, broader *N*-wave. In contrast, arrays IS42 and SJ1 on the other islands recorded two main signals with similar amplitudes (Figure 2b). The first signal arrived ~11 min after the earliest seismic arrival on São Miguel. The two occur two mins apart (125 s at SJ1; 103 s at IS42). These signals are more diffuse, longer in duration, lower in frequency (1.5–4 Hz), and weaker (maximum peak-to-peak amplitude ~1 Pa) than the signal on São Miguel. The arrival times of the

first signal align closely with the moveout of seismic arrivals from São Miguel and Terceira, with a velocity near the speed of sound in air (Figure 3).

We used a multi-channel cross-correlation method (Ulivieri et al., 2011), to determine back-azimuth and apparent velocity (Figure 2b; Figure S7 and S8 in Supporting Information S1). We processed 0.5–8 Hz bandpass filtered infrasound data, utilizing 5 s moving windows with 99% overlap. For IS42, the back-azimuths of the two arrivals are  $109.5^\circ (\pm 3.8^\circ)$  and  $109.1^\circ (\pm 5.1^\circ)$ . At SJ1, the back-azimuths are  $100.1^\circ (\pm 1.5^\circ)$  and  $99.0^\circ (\pm 2.0^\circ)$ . These back-azimuths align with a source located NE of São Miguel, consistent with the seismic arrivals and polarizations. Both arrays also show a weak third arrival with a back-azimuth like the preceding signals, approximately 2 minutes after the second arrival. Pressure-weighted mean velocities at IS42 and SJ1 are 350 and 320 m/s, respectively, with standard deviations of 8 m/s.

## 4. Source Location and Meteor Trajectory Model

### 4.1. Probabilistic Azimuth-Based Location

We estimated the source location using seismic horizontal polarization directions (Figure 1b) and back-azimuths from the first signal analyzed in the IS42 and SJ1 infrasound arrays (Figure 2b). To calculate the location probability density function (PDF), we considered the  $1\sigma$  back-azimuth uncertainties and computed PDFs for each back-azimuth on a 2-D grid. By multiplying these individual PDFs, we determined the maximum likelihood location and associated error ellipse (Stähler et al., 2022). Figure S2 in Supporting Information S1 displays the resulting PDF, while Figure 4a shows the 80% uncertainty ellipse. The primary source location uncertainty lies in the NW-SE direction, as the azimuth observations concentrate toward the West and SW due to network geometry and island geography. The maximum likelihood location lies approximately 42 km north-north-east (NNE) of the NE coast of São Miguel.

### 4.2. Constant Acoustic Velocity Source Model

Using a constant-velocity, straight-ray approximation, we derived a first-order source and trajectory model. This approach has been previously employed in studies of fireballs recorded by seismic networks (Che et al., 2016; Ishihara et al., 2003; Kumar et al., 2017; Yamada, 2021; Yamada & Mori, 2012). By optimizing the source parameters using the Genetic Algorithm (Kumar et al., 2017) and considering all recorded arrival times, we determined the origin time, 3-D source position, trajectory azimuth and inclination angle, and meteoroid velocity. To improve optimization, our polarization analysis results constrained the source position range (Table S1 in Supporting Information S1).

Our best-fitting solution has an overall root mean square (RMS) arrival time misfit of 2.6 s. The horizontally projected position closely aligns with the probabilistic location based on azimuths, falling within the 80% confidence interval (Figure 4a) and only 8 km from the maximum likelihood location. The source origin time is 02:02:38.8, with an elevation of 61 km, trajectory azimuth of  $250^\circ$ , and inclination of  $61^\circ$ . These initial parameters suggest that a meteoroid likely caused the observed seismoacoustic signals, rather than other possible sources such as an earthquake, quarry blast or thunderstorm. However, with the source lying outside our observation network, the trajectory parameters are weakly constrained, with interdependencies and tradeoffs among several parameters like elevation and origin time (Edwards et al., 2008; Yamada & Mori, 2012).

A more precise source position can be obtained using ray-tracing methods based on infrasound array data. However, these methods depend on an independently constrained origin time for the fireball (Belli et al., 2021).

### 4.3. Constraints From Satellite Data

Since the 2022 Azores meteoroid was not visually observed or captured on video, its timing and trajectory remain uncertain, causing tradeoffs with source position and limiting detailed analysis of the seismoacoustic data. To gather additional evidence, we examined data from the Geostationary Lightning Mapper (GLM) on the GOES-16 weather satellite. The GLM records transient light events at 500 fps with a resolution of 8–14 km (Rumpf et al., 2019). The minimum brightness detection is visual magnitude  $14\times$  (twice as bright as a full moon), so fireballs can be detected by the GLM (Jenniskens et al., 2018; Rumpf et al., 2019). We searched for flashes between 01:45 and 02:25 UTC on 2022/06/29,  $\sim 20$  min before and after our modeled source time (Figure S3 in Supporting Information S1). We identified a positive detection at 02:02:10.87. The GLM flash occurred 236 s before



the first seismic wave arrival at PM.BART, 28 s earlier and 93 km NE of our modeled source time using the constant-velocity, straight-ray approximation (Figure 4a). Infrared satellite data confirms minimal cloud cover in the area at the time, ruling out lightning as a source for the detection (Figure S1 in Supporting Information S1).

Since the Azores lie at the edge of GOES-16's line-of-sight coverage, we considered parallax errors in the geolocation of the flash. While automatically processed data from GLM considers parallax errors at typical lightning heights (up to 20–30 km at the edge of line-of-sight) (Virts & Koshak, 2020), emitters at greater heights, potentially including fireballs (Edwards et al., 2006; Gao & Mathews, 2015; Halliday et al., 1989), may see greater horizontal shifts (Rumpf et al., 2019). As the horizontal distance from the satellite subpoint increases, there is a higher chance that GLM will geolocate a flash farther away than its actual position (Virts & Koshak, 2020). We, therefore, calculated parallax corrections using *SatPy* (Raspaud et al., 2023) and found that source heights of 20–40 km matched the source position from the straight-ray modeling and polarisation analysis within 10 km distance (Figure 4a).

#### 4.4. Integrated Seismoacoustic-Satellite Source Model

Using the independently derived origin time from the GLM, we can reconstruct a more precise source position by employing 1-D ray-tracing in a realistic atmosphere velocity model (Belli et al., 2021). To create this model, we utilized 2.5° resolution data from the National Centers for Environmental Prediction and employed the AVOG2S software (Schwaiger et al., 2019) to extend climatological data up to the thermosphere. The velocity model is based on a 1-D vertical atmospheric profile (Figure S4 in Supporting Information S1) centered above Mosteiros on the West coast of São Miguel. The model consists of air temperature, air density and wind velocity, up to an altitude of 180 km (Figure S4 in Supporting Information S1). The model has a vertical resolution of 1 km in the first 20 km, and 2.5 km between 20 and 180 km.

From the infrasound back-azimuths and apparent velocities, we determined raypaths from the receiver back to the source. By comparing arrival times and the origin time from the GLM (02:02:10.87 UTC), the source position was calculated along the raypath (Belli et al., 2021). We applied this process separately for SJ1 and IS42 arrays, resulting in source positions only ~11 km apart (Figure 4a). The final source location is given as the average of these two positions: at 38.25°N, 24.86°W, 37.0 km altitude (11 km from the maximum likelihood azimuthal-based position), and <10 km away from the parallax-corrected flash position assuming an elevation of 27 km (Figure 4a). The difference in 10 km height is likely because source altitude is the most uncertain parameter of the source position modeling from infrasonic data. This spatial discrepancy may also result from a physical offset between the flash position and infrasound source along the meteoroid's trajectory. We then applied 3-D ray-tracing with *InfraGA* (Blom & Waxler, 2012) to this final source position to refine the raypaths and predict the arrival times at all stations that recorded the fireball event in São Miguel, Terceira, Graciosa and São Jorge (Figure 4b). Predictions are within ~10 s of all arrival time observations (Figures 3 and 4).

The 3-D raypaths (Figure 4b) demonstrate that the multiple signals at SJ1 and IS42 result from infrasonic multipathing from a single point source rather than multiple sources along the fireball trajectory. Seismic and infrasound arrivals on São Miguel are from direct stratospheric paths, while the weaker arrivals on Terceira are from rays guided by winds through the stratospheric waveguide (de Groot-Hedlin et al., 2011; Drob et al., 2003). The first infrasound arrivals at IS42 and SJ1 are also direct stratospheric-ducted rays. Conversely, secondary arrivals at IS42 and SJ1 are modeled as stratospheric-ducted rays with a surface reflection. Finally, the weak third infrasound arrival refracts at the base of the thermosphere (Figure 4b), where strong attenuation explains the low amplitude (Figure 2b) (Ott et al., 2021). Our raytracing model is not able to provide an explanation on the higher amplitude of the second arrival recorded at SJ1. The problem likely arises from the assumption a single 1-D atmospheric profile above São Miguel and therefore does not account for 3D small-scale atmospheric variations, which could explain such amplitude differences.

## 5. Discussion

### 5.1. Acoustic-Seismic Coupling Mechanisms

Seismic waveform characteristics on São Miguel, a relatively small island (~60 km long), exhibit substantial variability at short distances (Figures 1 and 2a). Although there was no clear correlation between known site properties,



the waveform variability due to different acoustic-to-seismic coupling properties must arise from multiple subtle site factors (Edwards et al., 2008; Hedlin & Walker, 2013; Kanamori et al., 1991; Stich et al., 2022). Monochromatic seismic waveforms (e.g., at CP.PVER) indicate air-coupled Rayleigh waves generated in a near-surface layer with a velocity slower than that of the air above (Albert et al., 2013; Anthony et al., 2022; Edwards et al., 2007). In contrast, weak precursory signals detected at PM.BART and PM.PGRON may represent coupled Rayleigh waves that form in a near-surface layer with a velocity faster than that of air (D'Auria et al., 2006; Edwards et al., 2008; Langston, 2004; Stich et al., 2022).

Initially, the colocated seismic and infrasound signals from IL.CMLA demonstrate relatively good coherence for  $\sim 0.6$  s (Figure S6 in Supporting Information S1). However, the infrasound signal is  $\sim 15$  s shorter, again emphasizing the role of local site effects. The absence of a  $\pi/2$  phase shift supports the presence of air-coupled Rayleigh waves rather than direct pressure loading from the atmosphere (Anthony et al., 2022). The relatively low coupling transfer coefficient (Edwards et al., 2007; Novoselov et al., 2020) of  $0.24 \mu\text{m/s/Pa}$  is consistent with the IL.CMLA's location on a higher-rigidity lava flow (Anthony et al., 2022), but is contrary to the expectation that weaker acoustic-seismic coupling restricts the generation of air-coupled Rayleigh waves (Wills et al., 2022).

### 5.2. Size of the 2022 Azores Fireball

An outstanding question remains about the size of the fireball. Brown et al. (2007) suggest  $\sim 6 \times 10^{-5}$  kt TNT equivalent as the minimum kinetic energy necessary for a meteoroid that is detectable by infrasound. To estimate the energy of the 2022 Azores fireball event, we used empirical relations (see e.g., Belli et al., 2021 and references therein). Our 3-D ray-tracing showed that the infrasound signal at IL.CMLA on São Miguel results from direct raypaths through the stratosphere. At such short distances, the most appropriate empirical relationship is the peak-to-peak amplitude size energy estimation of R. W. Whitaker (1995) that comes from explosion data sets, accounting for the wind speed along the raypath, and the horizontal distance between the source and receiver (Belli et al., 2021). With this relationship, we derive a kinetic energy of  $5.6 \times 10^{-3}$  kt TNT equivalent. For the more distant infrasound arrays on Graciosa (IS42) and São Jorge (SJ1), we used instead the period-based relationship of ReVelle (1997) that accounts for wind velocity encountered along the raypath and source-receiver distance. Applying this relationship to the signals, we estimate a similar kinetic energy of  $3.9 \times 10^{-3}$  kt TNT equivalent.

We can also use the luminous energy from the GLM-derived light curve (Figure S5 in Supporting Information S1) by converting luminous energy into visual magnitude and impact energy, accounting for the GLM pass-band and the altitude of the source. We follow the method described by Ott et al. (2021), adapted from Jenniskens et al. (2018). We estimate an energy of  $1.35 \times 10^{-4}$  kt TNT equivalent. This energy equates to a visual magnitude of  $-13.8$ , close to the previously hypothesized minimum detection threshold of the GLM (Rumpf et al., 2019). The energies derived from infrasound are about an order of magnitude larger than that from the GLM data. Ott et al. (2021) noted a similar discrepancy, and we speculate whether it relates to a physical difference in optical and acoustic energy release along the trajectory of meteoroids. Such systemic infrasound-optical energy discrepancies should be taken into account by future studies on fireballs that utilize lightning mapper data.

Applying this range in energy estimates to the power laws given by Brown, ReVelle, et al. (2002) and Brown, Spalding, et al. (2002), we estimate that the meteoroid's diameter was  $\sim 0.12$ – $0.40$  m. It is thought that approximately  $\sim 11,000$ – $400$  objects of this size typically enter Earth's atmosphere each year.

### 5.3. Implications for Fireball Detection

The flash was not identified as a fireball through automated processing of GLM data (Smith et al., 2021) or U.S. Government satellite data (<https://ceos.jpl.nasa.gov/fireballs/>) (Brown, Spalding, et al., 2002). In these automated detection pipelines, fireballs are identified by linear trajectories of individual flashes, and a light curve comprising greater energy release toward the end of the trajectory/flash event (Rumpf et al., 2019). However, from the locations of detection groups made up of individual events, there is no evidence for a systematic, linear trend in track, unlike other fireballs (Rumpf et al., 2019) (Figure S5 in Supporting Information S1). The 29 June 2022 event tracks over a small distance ( $< 1$  km), and the total flash duration is only 25 ms. Nor do we see a bias toward late energy disposition. These findings suggest that not all fireballs may conform to the characteristics identified by Rumpf et al. (2019). The lack of typical fireball source characteristics can be explained by parallax

errors along the satellite's line-of-sight at the edge of its field of view, especially if the object's trajectory was in the look direction of the satellite.

A remaining issue is why the 2022 Azores fireball was not seen or heard by humans, even though skies were clear (Figure S1 in Supporting Information S1). Time of day can bias observations, yet many previous fireballs have been seen and heard in the early hours (Ott et al., 2020). The most densely populated parts of São Miguel are on the South coast (e.g., the Ponta Delgada municipality and the neighboring areas; Figure 1b). In contrast, the fireball was located ~60 km NE of São Miguel, and large volcanic edifices in the center of the island may have partially obstructed the view of the fireball from the South.

## 6. Conclusions

Detailed seismoacoustic observations and modeling confirm a fireball source for the anomalous signal detected over the Azores in June 2022. The observed *W*-shapes in seismic waveforms are characteristic of a hypersonic or supersonic source. Array processing and 3-D ray-tracing of recorded infrasound pinpoint the terminal blast source at ~37 km altitude, ~60 km NE of São Miguel Island, consistent with seismic arrival times and polarization directions. Multiple infrasound signals are consistent with different raypath geometries and multipathing effects, rather than indicating distinct sources. Our observations are reinforced by recordings from a satellite-based lightning detector, which crucially provided a high-precision source origin time. To our knowledge, our studied event is a rare case of a fireball detected solely by a seismoacoustic network, rather than by human observers or *all-sky* cameras. The relatively weak energy of the event (~10<sup>-3</sup> kT TNT equivalent) and its associated small diameter (~0.1–0.4 m) challenge the typically assumed energy thresholds for the automated detection of fireballs from geophysical and satellite data. Thus, combining data from satellites and co-located seismoacoustic stations can increase the geographic and temporal detection completeness for such relatively small fireballs, thousands of which enter Earth's atmosphere annually. By increasing our observational coverage, this combination of data sources could thus help to better understand atmosphere entry processes of small near-Earth objects, and ultimately improve models of the structure of the atmosphere.

## Data Availability Statement

Windowed seismic waveforms cut out 50 s before and after the fireball signal are openly available in Hicks et al. (2023). Original seismic data from the IPMA network (code: PM) is available through IPMA's FDSN web service client (Instituto Português do Mar e da Atmosfera, 2006). Original seismic data from the Global Seismographic Network (GSN) station II.CMLA comes from the IRIS/EarthScope Data Management Center (Scripps Institution of Oceanography, 1986). Infrasound data from the SJ1 array of the Unifi network (code: FI) are available from Belli (2023). IMS data for the IS42 infrasound array are available on request from the CTBTO Preparatory Commission for scientific purposes through the virtual Data Exploitation Centre (vDEC). Original data from the GOES-16 Geostationary Lightning Mapper (GLM) was downloaded from NOAA's Comprehensive Large Array-data Stewardship System (CLASS). Infrared and cloud mask satellite data was obtained from EUMETSAT. *Code availability statement:* A Python Jupyter Notebook to reproduce the figures of this paper is available from Hicks et al. (2023). Seismic waveform data was processed using ObsPy (Krischer et al., 2015). Color palettes used for plotting come from the Scientific Color Maps package (Crameri, 2020; Crameri et al., 2020). Satellite data was processed using the PyGrib (J. Whitaker et al., 2020), SatPy (Raspaud et al., 2023), and GOES Python packages.

## References

- Albert, D. G., Taherzadeh, S., Attenborough, K., Boulanger, P., & Decato, S. N. (2013). Ground vibrations produced by surface and near-surface explosions. *Applied Acoustics*, 74(11), 1279–1296. <https://doi.org/10.1016/j.apacoust.2013.03.006>
- Anthony, R. E., Watzak, J., Ringler, A. T., & Wilson, D. C. (2022). Characteristics, relationships and precision of direct acoustic-to-seismic coupling measurements from local explosions. *Geophysical Journal International*, 230(3), 2019–2035. <https://doi.org/10.1093/gji/ggac154>
- Belli, G. (2023). Azores fireball infrasound data [Dataset]. OSF. <https://osf.io/987qv/>
- Belli, G., Pace, E., & Marchetti, E. (2021). Detection and source parametrization of small-energy fireball events in Western Alps with ground-based infrasonic arrays. *Geophysical Journal International*, 225(3), 1518–1529. <https://doi.org/10.1093/gji/ggab042>
- Blom, P., & Waxler, R. (2012). Impulse propagation in the nocturnal boundary layer: Analysis of the geometric component. *Journal of the Acoustical Society of America*, 131(5), 3680–3690. <https://doi.org/10.1121/1.3699174>

## Acknowledgments

AMG, SPH & MT acknowledge project UPFLOW which is funded by the Excellent Science programme of the European Research Council (Ref: 101001601). SBM is supported by the Fundação para a Ciência e Tecnologia (FCT) through the scholarship UI/BD/151384/2021. IVAR and CIVISA supported the installation and maintenance of the SJ1 infrasound array from the University of Florence on São Jorge Island. We thank Editor Germán A. Prieto, reviewer Jelle Assink, and an anonymous reviewer for their time and comments to improve our paper.

- Brown, P. G., Edwards, W. N., ReVelle, D. O., & Spurny, P. (2007). Acoustic analysis of shock production by very high-altitude meteors—I: Infrasonic observations, dynamics and luminosity. *Journal of Atmospheric and Solar-Terrestrial Physics*, 69(4), 600–620. <https://doi.org/10.1016/j.jastp.2006.10.011>
- Brown, P. G., Kalenda, P., Revelle, D. O., & Borovička, J. (2003). The Morávka meteorite fall: 2. Interpretation of infrasonic and seismic data. *Meteoritics & Planetary Sciences*, 38(7), 989–1003. <https://doi.org/10.1111/j.1945-5100.2003.tb00294.x>
- Brown, P. G., McCausland, P. J. A., Fries, M., Silber, E., Edwards, W. N., Wong, D. K., et al. (2011). The fall of the Grimsby meteorite—I: Fireball dynamics and orbit from radar, video, and infrasound records. *Meteoritics & Planetary Sciences*, 46(3), 339–363. <https://doi.org/10.1111/j.1945-5100.2010.01167.x>
- Brown, P. G., ReVelle, D. O., Tagliaferri, E., & Hildebrand, A. R. (2002). An entry model for the Tagish Lake fireball using seismic, satellite and infrasound records. *Meteoritics & Planetary Sciences*, 37(5), 661–675. <https://doi.org/10.1111/j.1945-5100.2002.tb00846.x>
- Brown, P. G., Spalding, R. E., ReVelle, D. O., Tagliaferri, E., & Worden, S. P. (2002). The flux of small near-Earth objects colliding with the Earth. *Nature*, 420(6913), 294–296. <https://doi.org/10.1038/nature01238>
- Cepelcha, Z., Borovička, J., Elford, W. G., ReVelle, D. O., Hawkes, R. L., Porubčan, V., & Šimek, M. (1998). Meteor phenomena and bodies. *Space Science Reviews*, 84(3), 327–471. <https://doi.org/10.1023/A:1005069928850>
- Che, I.-Y., Kim, G., & Lee, H.-I. (2016). Seismic and infrasonic analysis of the 9 March 2014 fireball in South Korea. *Geosciences Journal*, 20(2), 209–220. <https://doi.org/10.1007/s12303-015-0034-1>
- Cramer, F. (2020). Scientific colour maps [Software]. Zenodo. <https://doi.org/10.5281/zenodo.4153113>
- Cramer, F., Shephard, G. E., & Heron, P. J. (2020). The misuse of colour in science communication. *Nature Communications*, 11(1), 5444. <https://doi.org/10.1038/s41467-020-19160-7>
- D'Auria, L., Marotta, E., Martini, M., & Ricciolino, P. (2006). Seismic and acoustic detection of a bolide airburst in the Gulf of Naples (southern Italy). *Journal of Geophysical Research*, 111(B10), B10307. <https://doi.org/10.1029/2005JB004254>
- de Groot-Hedlin, C., Hedlin, M. A. H., & Walker, K. (2011). Finite difference synthesis of infrasound propagation through a windy, viscous atmosphere: Application to a bolide explosion detected by seismic networks. *Geophysical Journal International*, 185(1), 305–320. <https://doi.org/10.1111/j.1365-246X.2010.04925.x>
- Drob, D. P., Picone, J. M., & Garcés, M. (2003). Global morphology of infrasound propagation. *Journal of Geophysical Research*, 108(D21), 4680. <https://doi.org/10.1029/2002JD003307>
- Drolshagen, E., Ott, T., Koschny, D., Drolshagen, G., Schmidt, A. K., & Poppe, B. (2020). Velocity distribution of larger meteoroids and small asteroids impacting Earth. *Planetary and Space Science*, 184, 104869. <https://doi.org/10.1016/j.pss.2020.104869>
- Edwards, W. N., Brown, P. G., & ReVelle, D. O. (2006). Estimates of meteoroid kinetic energies from observations of infrasonic airwaves. *Journal of Atmospheric and Solar-Terrestrial Physics*, 68(10), 1136–1160. <https://doi.org/10.1016/j.jastp.2006.02.010>
- Edwards, W. N., Eaton, D. W., & Brown, P. G. (2008). Seismic observations of meteors: Coupling theory and observations. *Reviews of Geophysics*, 46(4), RG4007. <https://doi.org/10.1029/2007RG000253>
- Edwards, W. N., Eaton, D. W., McCausland, P. J., ReVelle, D. O., & Brown, P. G. (2007). Calibrating infrasonic to seismic coupling using the Stardust sample return capsule shockwave: Implications for seismic observations of meteors. *Journal of Geophysical Research*, 112(B10), B10306. <https://doi.org/10.1029/2006JB004621>
- Flinn, E. A. (1965). Signal analysis using rectilinearity and direction of particle motion. *Proceedings of the IEEE*, 53(12), 1874–1876. <https://doi.org/10.1109/PROC.1965.4462>
- Gao, B., & Mathews, J. D. (2015). High-altitude meteors and meteoroid fragmentation observed at the Jicamarca Radio Observatory. *Monthly Notices of the Royal Astronomical Society*, 446(4), 3404–3415. <https://doi.org/10.1093/mnras/stu2176>
- Halliday, I., Blackwell, A. T., & Griffin, A. A. (1989). The typical meteorite event, based on photographic records of 44 fireballs. *Meteoritics*, 24(2), 65–72. <https://doi.org/10.1111/j.1945-5100.1989.tb00946.x>
- Hedlin, M. A. H., Drob, D., Walker, K., & de Groot-Hedlin, C. (2010). A study of acoustic propagation from a large bolide in the atmosphere with a dense seismic network. *Journal of Geophysical Research*, 115(B11), B11312. <https://doi.org/10.1029/2010JB007669>
- Hedlin, M. A. H., & Walker, K. T. (2013). A study of infrasonic anisotropy and multipathing in the atmosphere using seismic networks. *Philosophical Transactions of the Royal Society A: Mathematical, Physical & Engineering Sciences*, 371(1984), 20110542. <https://doi.org/10.1098/rsta.2011.0542>
- Hicks, S., Matos, S., Pimentel, A., Belli, G., Gheri, D., Tsekhmistenko, M., et al. (2023). Supplementary Data and Codes for “Exclusive seismoacoustic detection and characterisation of an unseen and unheard fireball in the North Atlantic” by Stephen P. Hicks and Sandro B. Matos, et al [Dataset]. Zenodo. <https://doi.org/10.5281/zenodo.8226552>
- Hughes, A., Sankar, R., Davis, K. E., Palotai, C., & Free, D. L. (2022). Analysis of the April 13, 2021 bolide off the coast of Florida and Grand Bahama island. *Meteoritics & Planetary Sciences*, 57(3), 575–587. <https://doi.org/10.1111/maps.13781>
- Instituto Português do Mar e da Atmosfera, I.P. (2006). Portuguese national seismic network [Dataset]. International Federation of Digital Seismograph Networks. <https://doi.org/10.7914/SN/PM>
- Ishihara, Y., Tsukada, S., Sakai, S., Hiramatsu, Y., & Furumoto, M. (2003). The 1998 Miyako fireball's trajectory determined from shock wave records of a dense seismic array. *Earth Planets and Space*, 55(5), e9–e12. <https://doi.org/10.1186/BF03351752>
- Jenniskens, P., Albers, J., Tillier, C. E., Edgington, S. F., Longenbaugh, R. S., Goodman, S. J., et al. (2018). Detection of meteoroid impacts by the geostationary lightning mapper on the GOES-16 satellite. *Meteoritics & Planetary Sciences*, 53(12), 2445–2469. <https://doi.org/10.1111/maps.13137>
- Kanamori, H., Mori, J., Anderson, D. L., & Heaton, T. H. (1991). Seismic excitation by the space shuttle Columbia. *Nature*, 349(6312), 781–782. <https://doi.org/10.1038/349781a0>
- Krischer, L., Megies, T., Barsch, R., Beyreuther, M., Lecocq, T., Caudron, C., & Wassermann, J. (2015). ObsPy: A bridge for seismology into the scientific Python ecosystem. *Computational Science & Discovery*, 8(1), 014003. <https://doi.org/10.1088/1749-4699/8/1/014003>
- Kumar, U., Chao, B. F., Hsieh, Y., & Chang, E. T. Y. (2017). A meteor shockwave event recorded at seismic and infrasound stations in northern Taiwan. *Geoscience Letters*, 4(1), 13. <https://doi.org/10.1186/s40562-017-0079-2>
- Langston, C. A. (2004). Seismic ground motions from a bolide shock wave. *Journal of Geophysical Research*, 109(B12), B12309. <https://doi.org/10.1029/2004JB003167>
- Llorca, J., Trigo-Rodríguez, J. M., Ortiz, J. L., Docobo, J. A., García-Guinea, J., Castro-Tirado, A. J., et al. (2005). The villalbeta de la Peña meteorite fall: I. Fireball energy, meteorite recovery, strewn field, and petrography. *Meteoritics & Planetary Sciences*, 40(6), 795–804. <https://doi.org/10.1111/j.1945-5100.2005.tb00155.x>
- Novoselov, A., Fuchs, F., & Bokelmann, G. (2020). Acoustic-to-seismic ground coupling: Coupling efficiency and inferring near-surface properties. *Geophysical Journal International*, 223(1), 144–160. <https://doi.org/10.1093/gji/ggaa304>

- Ott, T., Drolshagen, E., Koschny, D., Drolshagen, G., Pilger, C., Gaebler, P., et al. (2021). Infrasound signals of fireballs detected by the Geostationary lightning mapper. *Astronomy & Astrophysics*, *654*, A98. <https://doi.org/10.1051/0004-6361/202141106>
- Ott, T., Drolshagen, E., Koschny, D., Drolshagen, G., Pilger, C., Mialle, P., et al. (2020). NEMO—The NEar real-time MONitoring system – Harvesting information online for a fireball monitoring and alert system. *Acta Astronautica*, *177*, 172–181. <https://doi.org/10.1016/j.actaastro.2020.07.013>
- Pujol, J., Rydelek, P., & Bohlen, T. (2005). Determination of the Trajectory of a fireball using seismic network data. *Bulletin of the Seismological Society of America*, *95*(4), 1495–1509. <https://doi.org/10.1785/0120040155>
- Pujol, J., Rydelek, P., & Ishihara, Y. (2006). Analytical and graphical determination of the trajectory of a fireball using seismic data. *Planetary and Space Science*, *54*(1), 78–86. <https://doi.org/10.1016/j.pss.2005.08.003>
- Raspaud, M., Hoese, D., Lahtinen, P., Holl, G., Finkensieper, S., Proud, S., et al. (2023). pytrill/satpy: Version 0.40.0 (2023/02/09) [Software]. Zenodo. <https://doi.org/10.5281/zenodo.7624532>
- Revelle, D. O. (1976). On meteor-generated infrasound. *Journal of Geophysical Research*, *81*(7), 1217–1230. <https://doi.org/10.1029/JA081i007p01217>
- ReVelle, D. O. (1997). Historical detection of atmospheric impacts by large Bolides using acoustic-Gravity waves a. *Annals of the New York Academy of Sciences*, *822*(1), 284–302. <https://doi.org/10.1111/j.1749-6632.1997.tb48347.x>
- Rumpf, C. M., Longenbaugh, R. S., Henze, C. E., Chavez, J. C., & Mathias, D. L. (2019). An Algorithmic approach for detecting Bolides with the Geostationary lightning mapper. *Sensors*, *19*(5), 1008. <https://doi.org/10.3390/s19051008>
- Schwaiger, H. F., Iezzi, A. M., & Fee, D. (2019). AVO-G2S: A modified, open-source ground-to-space atmospheric specification for infrasound modeling. *Computers & Geosciences*, *125*, 90–97. <https://doi.org/10.1016/j.cageo.2018.12.013>
- Scripps Institution of Oceanography. (1986). Global seismograph network—IRIS/IDA [Dataset]. International Federation of Digital Seismograph Networks. <https://doi.org/10.7914/SN/II>
- Silber, E. A., & Brown, P. G. (2014). Optical observations of meteors generating infrasound—I: Acoustic signal identification and phenomenology. *Journal of Atmospheric and Solar-Terrestrial Physics*, *119*, 116–128. <https://doi.org/10.1016/j.jastp.2014.07.005>
- Smith, J. C., Morris, R. L., Rumpf, C., Longenbaugh, R., McCurdy, N., Henze, C., & Dotson, J. (2021). An automated bolide detection pipeline for GOES GLM. *Icarus*, *368*, 114576. <https://doi.org/10.1016/j.icarus.2021.114576>
- Stähler, S. C., Zenhäusern, G., Clinton, J., & Giardini, D. (2022). Locating the Nordstream explosions using polarization analysis. *Seismica*, *1*(1). <https://doi.org/10.26443/seismica.v1i1.253>
- Stich, D., Casado Rabasco, J., Madiedo, J. M., Guerrero Rascado, J. L., & Morales Soto, J. (2022). Seismic observation and location of a meteor burst from a dense station deployment in southern Spain. *Geophysical Research Letters*, *49*(24), e2022GL099999. <https://doi.org/10.1029/2022GL099999>
- Tatum, J. B. (1999). Fireballs: Interpretation of airblast data. *Meteoritics & Planetary Sciences*, *34*(4), 571–585. <https://doi.org/10.1111/j.1945-5100.1999.tb01364.x>
- Ulivieri, G., Marchetti, E., Ripepe, M., Chiambretti, I., De Rosa, G., & Segor, V. (2011). Monitoring snow avalanches in Northwestern Italian Alps using an infrasound array. *Cold Regions Science and Technology*, *69*(2), 177–183. <https://doi.org/10.1016/j.coldregions.2011.09.006>
- Vera Rodriguez, I., Isken, M. P., Dahm, T., Lamb, O. D., Wu, S., Kristjánssdóttir, S., et al. (2022). Acoustic signals of a meteoroid recorded on a large-N seismic network and fiber-optic cables. *Seismological Research Letters*, *94*(2A), 731–745. <https://doi.org/10.1785/0220220236>
- Virts, K. S., & Koshak, W. J. (2020). Mitigation of geostationary lightning mapper geolocation errors. *Journal of Atmospheric and Oceanic Technology*, *37*(9), 1725–1736. <https://doi.org/10.1175/JTECH-D-19-0100.1>
- Walker, K. T., Hedlin, M. A. H., de Groot-Hedlin, C., Vergoz, J., Le Pichon, A., & Drob, D. P. (2010). Source location of the 19 February 2008 Oregon bolide using seismic networks and infrasound arrays. *Journal of Geophysical Research*, *115*(B12), B12329. <https://doi.org/10.1029/2010JB007863>
- Whitaker, J., Engle, E., Kemetmüller, J., van Kemenade, H., Zackrisson, M., Thorsteinsson, H., et al. (2020). jswhit/pygrib: Version 2.0.6 release. Zenodo. <https://doi.org/10.5281/zenodo.4292914>
- Whitaker, R. W. (1995). *Infrasonic monitoring*. Los Alamos National Lab. (LANL).
- Wills, G., Nippess, A., Green, D. N., & Spence, P. J. (2022). Site-specific variations in air-to-ground coupled seismic arrivals from the 2012 October 16 explosion at Camp Minden, Louisiana, United States. *Geophysical Journal International*, *231*(1), 243–255. <https://doi.org/10.1093/gji/ggac184>
- Yamada, M. (2021). Determining the source of the explosive sound heard in Hokkaido, Japan, on 26 April 2021. *Journal of Geophysical Research: Solid Earth*, *126*(12), e2021JB023076. <https://doi.org/10.1029/2021JB023076>
- Yamada, M., & Mori, J. (2012). Trajectory of the August 7, 2010 Bivako fireball determined from seismic recordings. *Earth Planets and Space*, *64*(1), 27–35. <https://doi.org/10.5047/eps.2011.08.021>